ISSN: 2664-9640

Design and Optimization of the Shape of a Single-person Submersible based on ANSYS

Miaomiao Xiu, Junhai Liu, Baolong Peng, Zhanbin Zhang

School of Shipping, Shandong Jiaotong University, Weihai, 264200, China

Abstract

Due to the complex growth environment of wild sea cucumbers, the difficulty and low efficiency of traditional ROV identification, at present, wild sea cucumber fishing is mainly obtained through manual fishing, in order to ensure the life safety of divers and improve the fishing efficiency of sea cucumbers, new ideas and solutions for single-man submersibles suitable for shallow water operations are proposed. Under the condition of ensuring the driver's operating space, the shape and structure of an easy-to-process manned submersible are designed to optimize its resistance performance. Creo was used to establish a model of a single-man submersible for shape design, and three design schemes were proposed: scheme 1 flat spindle type, scheme 2 imitation unmanned boat type, and scheme 3 imitation airfoil type. The drag performance of the single-man submersible is simulated and analyzed by using the Fluent module in the analytical fluid dynamics simulation software Ansys, and the results show that the drag performance of scheme 3 imitation airfoil type is better than that of other schemes.The conclusion was verified by simple experiments.It provides effective reference information for the subsequent structural optimization of single-man submersibles.

Keywords

Sea Cucumber Fishing; Single-man Submersible; Body-shape Design; Fluent.

1. Introduction

Due to the high nutritional and medicinal value of sea cucumbers, the global demand for sea cucumbers has increased year by year, and the cultivation area of sea cucumbers has gradually expanded, and the cultivation methods are also diverse, among which the sea cucumbers cultivated by bottom sowing method are infinitely close to wild sea cucumbers in terms of quality and nutritional value [1]. At present, the sea cucumber fishing method of bottom sowing culture can only be caught by divers, and this traditional fishing method has a high risk factor for divers and low fishing efficiency, which restricts the development of sea cucumber breeding industry. Therefore, new ideas and solutions for single-person submersibles suitable for shallow water operations are proposed.

Under the joint promotion of strong market demand and advanced technology progress, the development momentum of the manned submersible industry is strong. In 2018, research data from the Manned Submersibles Committee of the Association for Marine Technology [2] showed that there were 160 manned submersibles active in the world, providing 1,624 manned seats; Among them, 38 are used for submarine rescue and lifesaving, and 122 are used for scientific research, commercial operations, sightseeing, etc. In the direction of miniaturization and lightweight development of manned submersibles, foreign countries have more than 40 years of development experience. With the development of the world economy, small manned submersibles have become an indispensable choice for seabed tourism and marine ecosystem research. Its features: the use of fully transparent spherical manned cabin; the use of new materials to reduce the weight of the housing; The operating equipment is equipped with

ISSN: 2664-9640

modular design ideas, which is convenient for the update and upgrade of equipment in the future.

Although China started late in manned submersibles, after the development of science and technology and engineering technology during the "Eighth Five-Year Plan", "Ninth Five-Year Plan" and "Tenth Five-Year Plan", the technical level of China's manned submersibles [3] has been greatly improved. From the "Jiaolong" which was "ten years of project approval and ten years of development", to the "Deep Sea Warrior" that has repeatedly penetrated into the 10,000-meter deep-sea area for scientific research and exploration work, and then to the "Struggler" successfully sitting on the bottom of the Mariana Trench. In other areas, there is the "Huandao Jiaolong", which is used for underwater tourism, and the "Yulong", which is used for reservoir dam maintenance [4].

Manned submersibles can ensure the safety of divers and improve fishing efficiency, therefore, on the basis of existing research, the main goal of this design is to design an easy-to-process manned submersible under the condition of ensuring the pilot's operating space, optimize its resistance performance, and provide fast and agile response ability for underwater fishing and research.

2. The Shape Design of a One-man Submersible

Compared with deep-sea manned submersibles and manned sightseeing submersibles, shallow water single-person submersibles are very different in terms of shape, which is due to their different uses, working environments and design requirements. Its design is more compact for flexible operation and transport in shallow waters; The cockpit is usually small and only needs to accommodate a single person, providing basic visibility and operating space; The operation interface is designed to be simple and easy to be operated by a single person; Pay attention to fluid dynamics, reduce underwater resistance, The key technical parameters, as shown in Table 1, and the overall design scheme, as shown in Figure 1, include the overall shape and structure design, electrical design, control design and safety design.

Table 1. Key technical parameters

Physical Dimensions/mm	Maximum Withstand Voltage Depth/m	Maximum Sailing Speed / (Kn/h)	Maximum Endurance/h
2800*800*400	50	3	5

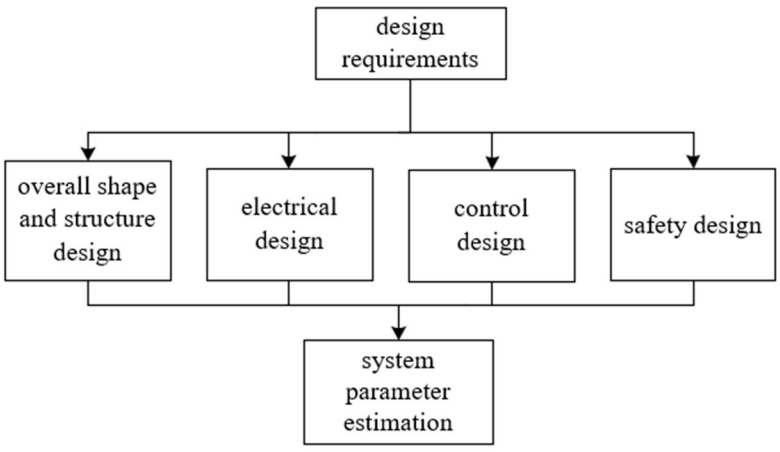

Figure 1. Design scheme of a single-person submersible

ISSN: 2664-9640

The shape design of the single-person submersible mainly considers that the main body can adapt to the growth environment of 20-meter underwater sea cucumber, but the situation of the ocean is complex and unpredictable, so the limit depth of the designed single-person submersible is 50 meters. The size design of the manned submersible is based on a human model with a height of 180cm and a weight of 80kg as a reference, and has a complete life detection system, a dynamic balance control system, a control system of various sensors and a power system built-in, and the specific internal structure is shown in Figure 2, and the equipment and load are reasonably arranged to ensure that the center of gravity is near the center of buoyancy.

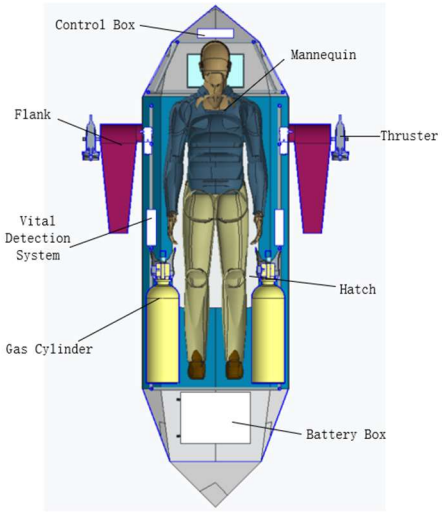

Figure 2. Internal layout of single-man submersible

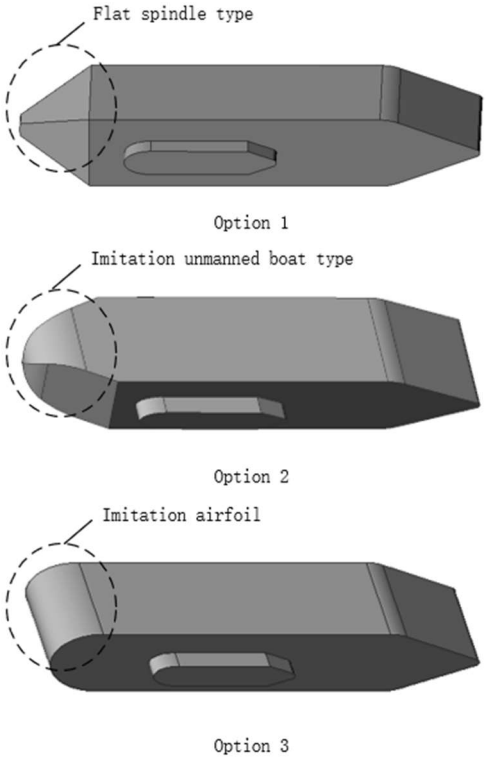

Figure 3. 3D Simplified Appearance of Single Submarine

ISSN: 2664-9640

The preliminary scheme of the overall shape design of the single-person submersible is a flat spindle type, with a large slender-to-length ratio, flanks on both sides, and a built-in device for fishing sea cucumbers, which can not only reduce the navigation resistance, but also ensure the stability of navigation. According to the bow of the unmanned boat, scheme 2 is proposed to imitate the unmanned boat type and increase the streamlined shape of the bow. Scheme 3 imitates the airfoil [5], which is similar to the streamlined profile of an aircraft wing, reduces turbulence and drag, and the internal rib design is reinforced to enhance the compressive performance, and the three-dimensional simplified shape of the single-person submersible is shown in Figure 3.

3. Fluent Hydrodynamic Analysis

3.1. Computational Models and Meshing

The computational domain setting [6] is a cylindrical area: the diameter is 5D, the inlet surface is 1.5 L away from the front of the single submersible, and the outlet surface is 3.5 L away from the tail, where D is the maximum width of the single submersible and L is the total length of the single submersible, as shown in Figure 4.

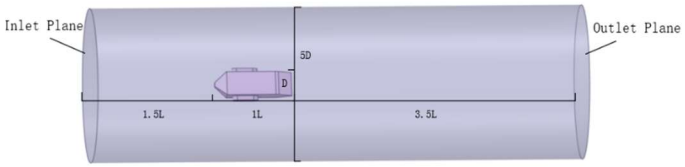

Figure 4. Schematic diagram of Fluent computational domain

Boundary conditions are set: the inlet boundary condition is the velocity inlet boundary condition, the outlet is the pressure outlet boundary condition, the side is the wall boundary condition, and the one-man submersible is the wall no slip boundary condition, and the default value of the subrelaxation factor is used to calculate the initial field.

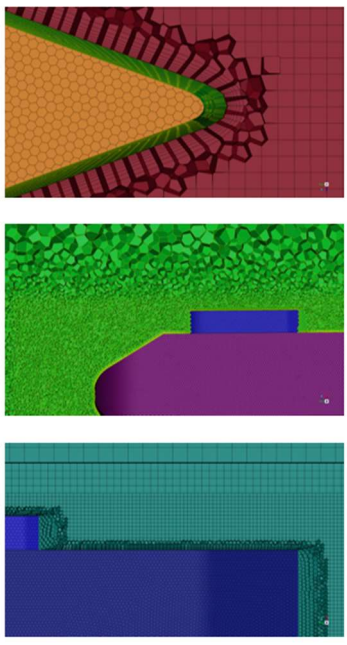

Figure 5. Parts of the mesh detail

ISSN: 2664-9640

Fluent (includes CFD-Post) software is used for meshing, and Fluent Meshing meshing adopts a polyhedral solution, which has the characteristics of small number of meshes, relatively high computing efficiency, calculation accuracy and mesh quality. The total number of simplified model meshes of the single-person submersible is 844,700, 970,100 and 770,200, respectively, and some of the mesh details are shown in Figure 5.

3.2. Governing Equation

From the perspective of Newtonian mechanics, since water is usually considered to be an incompressible viscous fluid, the flow must follow the laws of conservation of mass and momentum.

Ref. [7] gives the following general form,

$$\frac{\partial(\rho\varphi)}{\partial t} + \nabla(\rho u \emptyset\varphi) = \nabla(\Gamma\Delta\varphi) + S \tag{1}$$

where: φ is a generic variable; Γ is the generalized diffusion coefficient; S is a generalized source term. When φ= 1,Γ=0,S=0, the equation is a continuity equation, and when $\varphi = u_i$,Γ= μ, the $S = -\frac{\partial p}{\partial x_i} + S_i$,equation is a momentum equation.

3.3. Turbulence Model

The standard $k-\varepsilon$ model has good robustness and economy, and has reasonable accuracy for various turbulent flows, while the Realizable $k-\varepsilon$ model [8] derives ε the modified transport equation of the dissipation rate based on the exact equation of the mean square vorticity fluctuation, and is superior to the standard $k-\varepsilon$ model in terms of rotational uniform shear flow, jet, free flow in mixed layers, channel and boundary layer flow, and separated flow. In this paper, the Realizable $k-\varepsilon$ turbulence model is used for the simulation model.

The Realizable $k-\varepsilon$ model equations are:

$$\begin{cases} \frac{\partial(\rho k)}{\partial t} + \frac{\partial(\rho k \cdot u_j)}{\partial x_j} = \frac{\partial}{\partial x_j}\left[\left(\mu + \frac{\mu_t}{\sigma_k}\right)\cdot\frac{\partial k}{\partial x_j}\right] + G_k + G_b - \rho\varepsilon - Y_m + S_k \\ \frac{\partial(\rho\varepsilon)}{\partial t} + \frac{\partial(\rho u_j \varepsilon)}{\partial x_j} = \frac{\partial}{\partial x_j}\left[\left(\mu + \frac{\mu_t}{\sigma_k}\right)\cdot\frac{\partial \varepsilon}{\partial x_j}\right] + \rho C_1 S\varepsilon - \rho C_2 \frac{\varepsilon^2}{k+\sqrt{v\varepsilon}} + C_{1\varepsilon}\frac{\varepsilon}{k}C_{3\varepsilon}G_b + S_\varepsilon \end{cases} \tag{2}$$

where: k is the turbulent energy, is the μ_t turbulent viscosity; S_k and S_ε are source terms, respectively; G_k is the turbulent energy caused by the average velocity gradient, and the turbulent viscosity μ_t establishes a functional relationship through the variables ε, and determines the relationship between the two variables, whose relationship is:

$$\mu_t = \rho C_\mu \frac{k^2}{\varepsilon} \tag{3}$$

where: C_μ is the empirical constant; ε is the turbulent dissipation rate.

3.4. Calculation Results and Analysis

3.4.1. Numerical Simulation and Analysis of Three Shape Design Schemes

When the single-person submersible designed by Fluent software is used to analyze the resistance of the one-man submersible when it travels in the horizontal direction underwater, the resistance direction is opposite to the direction of sailing. When a one-man submersible sails underwater at 2.5 m/s, the pressure distribution is shown in Figure 6, and the change in velocity is shown in Figure 7.

ISSN: 2664-9640

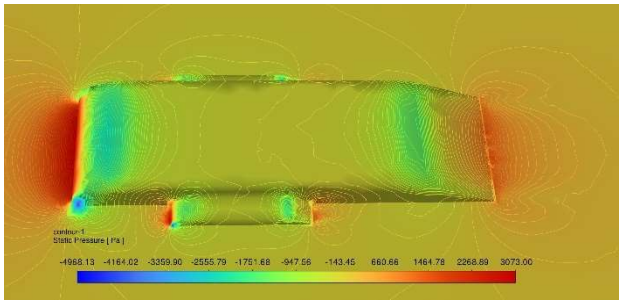

Figure 6. Single-man submersible 2.5m/s pressure contour

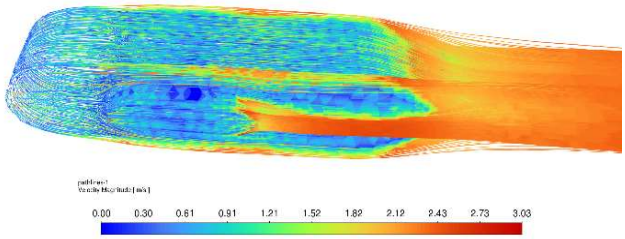

Figure 7. Single-man submersible 2.5m/s velocity pathline

For the three design schemes proposed above, the sailing resistance of the single-person submersible at different sailing speeds, as shown in Table 2, the sailing resistance line chart, shown in Figure 8.

By comparing the resistance values of Option 2, Option 3 and Option 1 respectively, the resistance values of Option 2 are greater than the resistance values of Option 1, and the increase is about 26%; The resistance value of Option 3 is smaller than that of Option 1, and the decrease is about 77%. According to the resistance equation proposed by Lord Rayleigh, the resistance $C_d = \frac{F_d}{0.5\rho v^2 A}$coefficient of Option 2 is about 26% greater than that of Option 1, and the resistance coefficient of Option 3 is about 77% less than that of Option 1, so the resistance performance of Option 3 is the best, better than Option 1 and Option 2.

Table 2. Sailing speed and the corresponding resistance

Speed m/s	Option 1	Option 2	Option 3	Amplification 1	Amplification 2
0.5	0.14	0.19	0.04	38%	-73%
1	0.62	0.81	0.15	29%	-76%
1.5	1.46	1.86	0.33	27%	-77%
2	2.68	3.36	0.57	26%	-79%
2.5	4.22	5.30	1.08	26%	-74%
3	6.11	7.66	1.36	25%	-78%
3.5	8.43	10.53	1.89	25%	-78%
4	10.89	13.83	2.46	27%	-77%

Note: 1. The increase of 1 refers to the percentage increase of the corresponding resistance value of Option 2 compared with Option 1;

2. Amplification 2 refers to the percentage increase in the corresponding resistance value of Option 3 compared with Option 1.

ISSN: 2664-9640

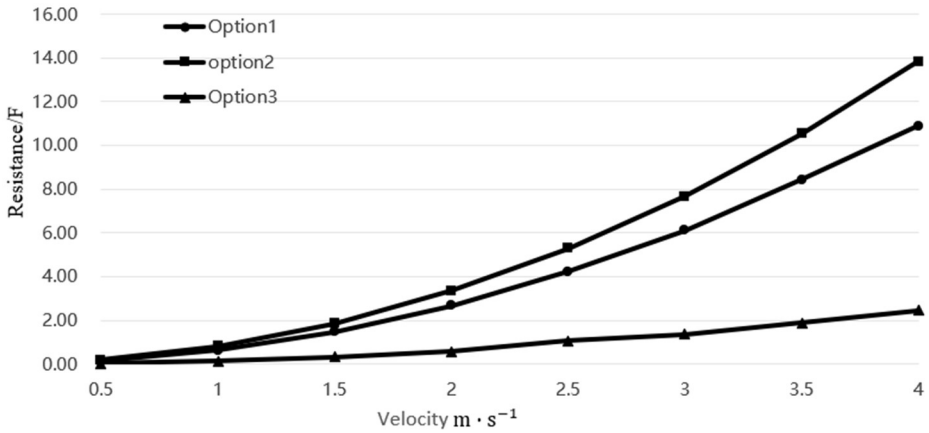

Figure 8. Line chart of sailing resistance

3.4.2. Flow Field Fractions During the Calculation Process

Result analysis: From the flow field distribution shown in Figure 9-11, it can be clearly seen that the tail flow field of scheme 3 is more uniform than that of scheme 1 and scheme 2, so it can be inferred that scheme 3 is more conducive to the propeller propulsion efficiency.

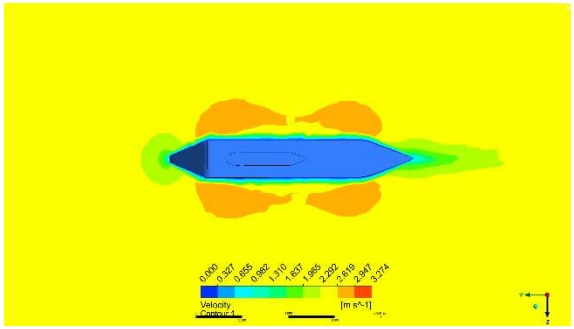

Figure 9. Option 1 2.5m/s schematic diagram of the flow field distribution

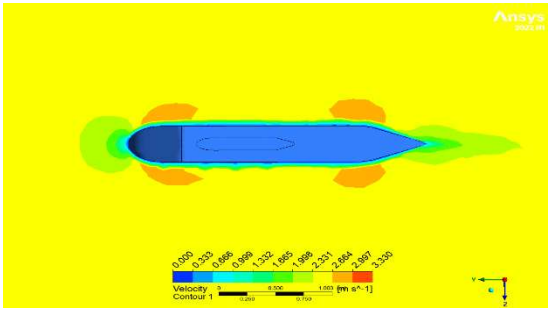

Figure 10. Option 2 2.5m/s schematic diagram of the flow field distribution

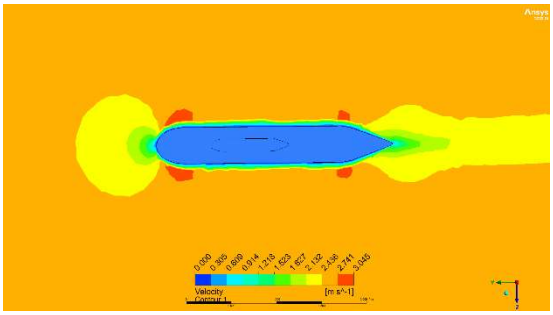

Figure 11. Option 3 2.5m/s schematic diagram of the flow field distribution

ISSN: 2664-9640

4. Experimental Verification

The three scheme models of this design are 3D printed at a scale of 1:10, as shown in Figure 12, using a tensile force gauge with a load index value of 0.1N, and the resistance is roughly measured under the same water flow, and the test scene is shown in Figure 13, and the specific resistance value is shown in Table 3.

Figure 12. 3D models

Table 3. Resistance

Option1	Option2	Option3
7.2	11.2	4.1

Figure 13. Test Scenarios

5. Conclusion

In the results of horizontal navigation of the single-person submersible, by comparing the calculated values of the drag coefficient of the three schemes, it is found that the drag performance of scheme 3 is the best, and by comparing the calculation results of the flow field, it is found that the tail flow field of scheme 3 is better than that of scheme 1 and scheme 2, which is more conducive to the propulsion efficiency of the propeller. In this paper, the Fluent simulation method is used to compare some of the hydrodynamic properties of the three schemes, and it is concluded that the drag performance of scheme 3 imitation airfoil is better than that of other schemes.

Through the simple underwater test, the 3D model is kept stable at a certain water depth under the same water flow velocity, and the resistance performance of scheme 3 is better than that of other schemes. In the future work, the hydrodynamic performance of other aspects can be further compared, and the design scheme can be improved, and the next step should be considered to meet the specific design parameters and realize the basic function; According to the actual situation, the electrical layout is carried out, and the corresponding sensors are equipped to realize specific functions.

ISSN: 2664-9640

References

[1] Research on sea cucumber mariculture technology[J]. Wang Rusheng. Livestock and poultry industry, 2019(09).

[2] William K. MTS manned underwater vehicles 2017-2018 global industry overview [J]. Marine Technology Society Journal, 2018, 52(5): 125–151.

[3] Hu Zhen,Cao Jun. Development and application of manned deep diving technology[J]. Strategic Study of Chinese Academy of Engineering, 2019, 21(6): 87-94.

[4] Wang Lei,Hu Zhonghui,Jiang Lei, et al. Design and development of special submersible for deep-water detection of Yulong Dam[J]. Chinese Shipbuilding, 2022,63(05):157-166.

[5] Wang Qing,Zhang Min,Li Deshun, et al. Optimized design of wind turbine airfoil shape based on low-speed pretreatment[J]. Acta Solaria Sinica, 2022,43(05):351-358.

[6] Feng Kangjia,Hu Fanglin,Liu Le. Analysis of influencing factors of CFD simulation of plane motion mechanism test[J]. Ship Engineering,2020,42(04):44-48.

[7] Zou Lei,Tian Wei,Lin Yuan, et al. Study on the hydrodynamic characteristics of propellers based on different turbulence models[J]. Ship Engineering, 2023,45(12):94-100+114.

[8] Liu Fanghua,Yao Rao. Analysis of hydrodynamic performance of unmanned underwater vehicles[J]. Ship Science and Technology,2022,44(12):76-82.